

# Coupled waveguide modes in hexagonal photonic crystals

J. Scott Brownless,<sup>1,\*</sup> Sahand Mahmoodian,<sup>1</sup> Kokou B. Dossou,<sup>2</sup>  
Felix J. Lawrence,<sup>1</sup> Lindsay C. Botten,<sup>2</sup> and C. Martijn de Sterke<sup>1</sup>

<sup>1</sup>*IPOS and CUDOS, School of Physics, University of Sydney, 2006, Australia*

<sup>2</sup>*CUDOS, School of Mathematical Sciences, Univ. of Technology, Sydney, 2007, Australia*

[\\*jbro@physics.usyd.edu.au](mailto:*jbro@physics.usyd.edu.au)

**Abstract:** We investigate the modes of coupled waveguides in a hexagonal photonic crystal. We find that for a substantial parameter range the coupled waveguide modes have dispersion relations exhibiting multiple intersections, which we explain both intuitively and using a rigorous tight-binding argument.

© 2010 Optical Society of America

**OCIS codes:** (130.5296) Photonic crystal waveguides.

---

## References and links

1. S. Kubo, D. Mori, and T. Baba, "Low-group-velocity and low-dispersion slow light in photonic crystal waveguides," *Opt. Lett.* **32**, 2981–2983 (2007).
2. A. Y. Petrov and M. Eich, "Zero dispersion at small group velocities in photonic crystal waveguides," *Appl. Phys. Lett.* **85**, 4866–4868 (2004).
3. A. A. Sukhorukov, A. V. Lavrinenko, D. N. Chigrin, D. E. Pelinovsky, and Y. S. Kivshar, "Slow-light dispersion in coupled periodic waveguides," *J. Opt. Soc. Am. B* **25**, C65–C74 (2008).
4. D. Mori and T. Baba, "Dispersion-controlled optical group delay device by chirped photonic crystal waveguides," *Appl. Phys. Lett.* **85**, 1101–1103 (2004).
5. A. Martinez, F. Cuesta, and J. Marti, "Ultrashort 2-D photonic crystal directional couplers," *IEEE Photon. Technol. Lett.* **15**, 694–696 (2003).
6. Y. A. Vlasov, M. O'Boyle, H. F. Hamann, and S. J. McNab, "Active control of slow light on a chip with photonic crystal waveguides," *Nature* **438**, 65–69 (2005).
7. P. Yeh, *Optical Waves in Layered Media* (Wiley, New York, 1988). Chap. 11.
8. K. Iizuka, *Elements of Photonics, Volume II* (Wiley, 2002). Chap. 9.
9. C. M. de Sterke, L. C. Botten, A. A. Asatryan, T. P. White, and R. C. McPhedran, "Modes of coupled photonic crystal waveguides," *Opt. Lett.* **29**, 1384–1386 (2004).
10. A. Locatelli, M. Conforti, D. Modotto, and C. D. Angelis, "Discrete negative refraction in photonic crystal waveguide arrays," *Opt. Lett.* **31**, 1343–1345 (2006).
11. S. Ha, A. A. Sukhorukov, K. B. Dossou, L. C. Botten, A. V. Lavrinenko, D. N. Chigrin, and Y. S. Kivshar, "Dispersionless tunneling of slow light in antisymmetric photonic crystal couplers," *Opt. Express* **16**, 1104–1114 (2008).
12. A. A. Sukhorukov, S. Ha, A. S. Desyatnikov, A. V. Lavrinenko, and Y. S. Kivshar, "Slow-light vortices in periodic waveguides," *J. Opt. A, Pure Appl. Opt.* **11**, 094016 (2009).
13. L. C. Botten, K. B. Dossou, S. Wilcox, R. C. McPhedran, C. M. de Sterke, N. A. Nicorovici, and A. A. Asatryan, "Highly accurate modelling of generalized defect modes in photonic crystals using the FSS method," *Int. J. Microwave Opt. Technol.* **1**, 133–145 (2006).
14. F. S. Chien, Y. Hsu, W. Hsieh, and S. Cheng, "Dual wavelength demultiplexing by coupling and decoupling of photonic crystal waveguides," *Opt. Express* **12**, 1119–1125 (2004).
15. S. Mahmoodian, C. G. Poulton, K. B. Dossou, R. C. McPhedran, L. C. Botten, and C. M. de Sterke, "Modes of shallow photonic crystal waveguides: semi-analytic treatment," *Opt. Express* **17**, 19629–19643 (2009).
16. K. B. Dossou, C. G. Poulton, L. C. Botten, S. Mahmoodian, R. C. McPhedran, and C. Martijn de Sterke, "Modes of symmetric composite defects in two-dimensional photonic crystals," *Phys. Rev. A* **80**, 013826 (2009).

17. L. C. Botten, N. A. Nicorovici, R. C. McPhedran, C. M. de Sterke, and A. A. Asatryan, "Photonic band structure calculations using scattering matrices," *Phys. Rev. E* **64**, 046603 (2001).
18. L. C. Botten, T. P. White, A. A. Asatryan, T. N. Langtry, C. M. de Sterke, and R. C. McPhedran, "Bloch mode scattering matrix methods for modeling extended photonic crystal structures. I. theory," *Phys. Rev. E* **70**, 056606 (2004).
19. L. C. Botten, R. A. Hansen, and C. M. de Sterke, "Supermodes in multiple coupled photonic crystal waveguides," *Opt. Express* **14**, 387–396 (2006).

## 1. Introduction

Coupled photonic crystal waveguides (CPCWs) have received substantial attention due to their ability to guide slow light with significant control over dispersion [1–3]. The unique properties of CPCWs have led to high bandwidth delay lines [4] and directional couplers with extremely short coupling lengths [5] needed to create ultra compact devices [6]. Analysis of the underlying coupled waveguide modes (CWMs) is critical to understanding how these properties are achieved. Coupled waveguides in uniform media are well understood: the fundamental mode is always even, the second mode is odd [7, 8] and the dispersion curves of the two modes do not cross. de Sterke *et al.* [9] showed that the fundamental CWM of square lattice PCWs can be either even or odd, and that this depends on the number of rows between the waveguides. Since the coupling coefficient is given by  $C = (\beta_{\text{even}} - \beta_{\text{odd}})/2$ , the existence of an odd fundamental CWM in square photonic crystals (PCs) led to the realisation of structures with negative coupling coefficients exhibiting discrete negative refraction [10].

There are key differences between square and hexagonal lattice CPCWs which make the hexagonal case a more interesting, and ultimately more challenging, problem to study. First, there exist two distinct geometries for coupled waveguides, the *inline* case with an odd number of rows between PCWs [inset Fig. 1(b)], and the *staggered* case with an even number of rows between PCWs [inset in Fig. 1(a)]. The inline case has reflection symmetry since the centers of the cylinder defects in the two waveguides line up. No such symmetry exists for the staggered case as the cylinder centers do not line up. The two waveguide configurations exhibit different behaviour at the Brillouin zone (BZ) edge. Figure 1 shows that in the staggered arrangement, the even and odd dispersion curves intersect at the BZ edge, while they are well separated in the inline configuration. This behaviour was reported previously [11, 12], and has resulted in

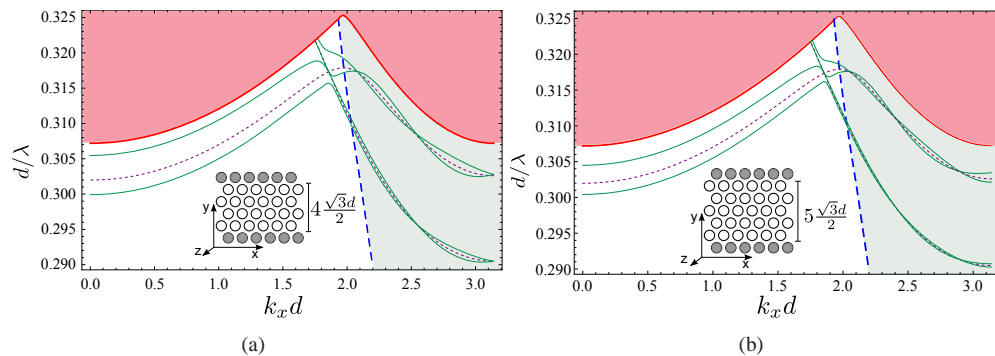


Fig. 1. Dispersion curves of CWMs for (a) PCWs separated by four rows (staggered geometry) and (b) PCWs separated by five rows (inline geometry). The purple dashed curve and the solid green curves are for a single waveguide and for CPCWs, respectively. The red shaded area indicates the projected bands and the green area is the braided region, separated from the typical region by the blue dashed curve.

staggered CPCWs being proposed for use as slow light couplers [11].

Here, we take a more general interest in CWMs in hexagonal lattices. We consider a PC with a background index of  $n_b = 3$ , air holes of radius  $r_c = 0.3d$ , where  $d$  is the period, and use  $H_z$  polarisation. We create the PCWs by altering the refractive index of rows of holes to  $n_d = 1.5$ . Figure 1 shows that for both the inline and staggered geometries, the dispersion curves, which were computed using the generalised fictitious source superposition method [13], differ on either side of the dashed blue curve. We refer to the area to the right of this curve (green background) as the *braided* region as the dispersion curves of the coupled modes are interwoven around the single waveguide mode leading to multiple degeneracies. At these degeneracies the PCW modes do not couple. Such a point in the dispersion curve can be used to design compact demultiplexers [14]. The presence of the braiding means that the coupling coefficient depends not only on the geometry of the system but also depends strongly on the Bloch wavevector  $k_x$ . The degeneracies here are not accidental, but are associated with how the mode of the PCW decays in the bulk PC separating the waveguides. We refer to the region to the left of this curve as *typical*, since the modes display similar properties to those in a square lattice.

Unlike square lattices, where the symmetry of the fundamental mode depends on the spacing between the waveguides, the symmetry of the fundamental mode in hexagonal lattice CWMs changes both with the spacing and with the Bloch wavevector, *i.e.* the symmetry of the fundamental mode varies across the BZ. As the spacing between the waveguides increases by two rows an extra crossing appears within the braided region. In this paper we analyse the intricacies of CWMs in hexagonal CPCWs. We do this in Section 2 by providing a physical argument as to why such degeneracies should exist inside the BZ, and explain how they depend on the parameters of the CPCWs and the underlying bulk PC. In Section 3 we provide a rigorous analysis of the CWMs using a perturbative method based on the modes of the single uncoupled PCW. We discuss our results in Section 4. The Appendix provides some proofs for Section 2.

## 2. Physical Argument

Deep inside the band gap, the interaction between waveguides is weak, allowing us to use a tight binding approximation. In this regime, the splitting of the coupled modes occurs symmetrically around the single waveguide mode. This splitting is proportional to the  $J$  overlap integral [7],

$$J = \int \delta\epsilon \mathbf{E}_1(\mathbf{r}) \cdot \mathbf{E}_2^*(\mathbf{r}) d^2\mathbf{r} = \int \delta\epsilon (E_{x1}(\mathbf{r})E_{x2}^*(\mathbf{r}) + E_{y1}(\mathbf{r})E_{y2}^*(\mathbf{r})) d^2\mathbf{r}. \quad (1)$$

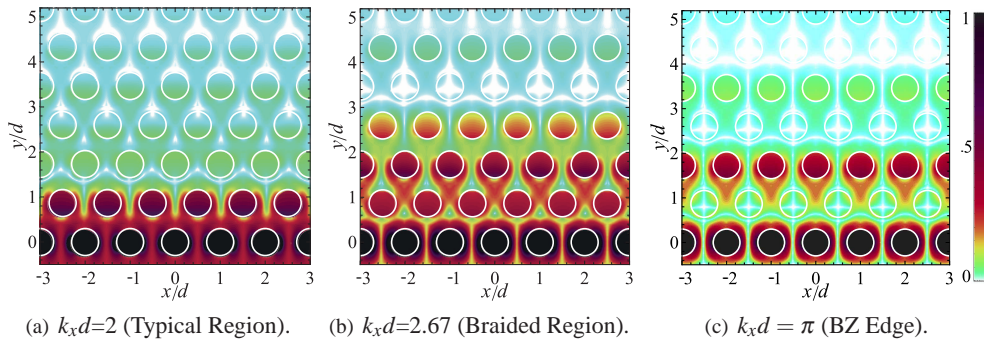


Fig. 2.  $|E_y|$  fields of the even single PCW mode for a PCW centered at  $y = 0$ . The scale has been chosen so as to emphasize the weak fields which are involved in coupling the PCWs. The value of  $k_x d$  for Fig. 2(b) corresponds to a crossing at spacing 4.

Here  $\delta\epsilon$  is the perturbation formed by one of the waveguides. For the PCW mode that has a  $H_z$  field that is even (odd) with respect to its center, there is a nodal line at the center of the PCW for the  $E_x$  ( $E_y$ ) component, so the dominant contribution to the splitting is from the  $E_y$  ( $E_x$ ) component. This means that the magnitude of the coupling depends on only one field component of the single PCW mode.

Figure 2 shows the relevant electric field for the even mode of a PCW, situated at  $y = 0$ . When moving away from the waveguide in the braided region, the field has nodal lines (at four rows away in Fig. 2(b) and at one, three and five rows away in 2(c)). If the second waveguide is situated on such a nodal line the waveguide coupling is small and their dispersion curves intersect. In the typical region [Fig. 2(a)] the envelope of the field simply decays exponentially in  $y/d$  and intersections do not occur. In the braided region [Fig. 2(b)] the mode decays exponentially but with an underlying periodic feature, the novel element considered here.

The nature of this decay is best explained by considering the complex bands of the bulk PC. The complex bands arise by finding the  $\mathbf{k}$  values, real or complex, associated with a real frequency. Since complex bands are continuous when the frequency is varied, a bandgap can be considered to be a frequency interval with only complex bands but no real ones. PCWs are periodic in  $x$  therefore their modes propagate with a fixed value of a (real)  $k_x$ . When describing how the modes decay in the bulk we thus choose to make  $k_y$  complex while keeping  $k_x$  real. The modes of a bulk PC are Bloch modes which acquire a Bloch factor  $\mu$  after translation along a lattice vector. For a propagating Bloch mode  $|\mu| = 1$ , while for an evanescent solution  $|\mu| < 1$ . For this lattice we define the lattice vector,  $\mathbf{e}_2 = [d/2, d\sqrt{3}/2]$ , shown in Fig. 5(a). When translating along the lattice vector  $-\mathbf{e}_2$ , the Bloch factor is given by  $\mu = e^{-i\mathbf{k}\cdot\mathbf{e}_2}$ , and thus the imaginary part of the Bloch vector  $\mathbf{k}$  denotes the decay rate.

The complex band diagrams shown in Fig. 3 are for three different values of  $k_x d$ , with the color representing decay rate of the Bloch mode: Fig. 3(a) is for  $k_x d = 0.31$  in the typical region, (b) is for  $k_x d = 2.51$ , in the typical region for  $d/\lambda < 0.2531$  and in the braided region for  $d/\lambda > 0.2531$ , while (c) is at the BZ edge and completely within the braided region. Figure 3(b) and 3(c) show that in the braided region there are two equally dominant evanescent Bloch modes. The presence of either one or two dominant evanescent Bloch modes defines the typical and braided regions respectively. The line separating these regions in Fig. 1 corresponds to the bifurcation point in the complex band-structure. This extends the work of Mahmoodian *et al* [15] to complex bands.

To illustrate the behaviour of the bands within the braided region, we consider how the field

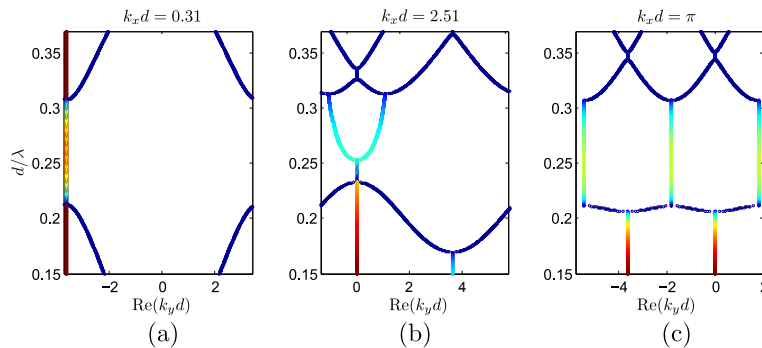


Fig. 3. Complex band diagrams at different slices of  $k_x$  for the bulk hexagonal lattice. Dark blue indicates real bands, while other colours indicate complex bands. (a)  $k_x d$  is in the typical region; (b)  $k_x d$  intersects the blue dashed curve in Fig. 1; (c)  $k_x d$  is at the BZ edge.

decays along lattice vectors in the bulk PC. As shown in Fig. 3 in the braided region, for a given value of  $k_x$  there are two complex Bloch modes with the same decay rate,  $\kappa$ , with opposite signs of  $\text{Re}(k_y)$  (which we refer to as  $k_y$ ). Thus, when translating  $m$  times by the bulk lattice vector  $-\mathbf{e}_2$ , we acquire a Bloch factor

$$\mu_{\pm}^m = e^{-im\mathbf{k}\cdot\mathbf{e}_2} = e^{-ik_x md/2} e^{\pm ik_y md\sqrt{3}/2} e^{-\kappa md\sqrt{3}/2}, \quad (2)$$

where  $k_y$  refers to the real part of the Bloch vector. Since we are interested in coupled PCW modes we assume the single PCW mode has been computed and analyze how the mode decays in the bulk. As described in the Appendix, we can write the single PCW mode in the bulk region as a superposition of the decaying bulk Bloch modes,  $\varphi_i$ . In the braided region there are two leading order Bloch modes which decay at the same rate. We ignore all but these modes. Taking their amplitudes as  $c_1$  and  $c_2$ , after decaying along  $m$  lattice vectors the field of the PCW is

$$\begin{aligned} \psi(\mathbf{r}_0 + m\mathbf{e}_2) = & c_1 \varphi_1(\mathbf{r}_0) e^{-ik_x md/2} e^{-ik_y md\sqrt{3}/2} e^{-\kappa md\sqrt{3}/2} + \\ & c_2 \varphi_2(\mathbf{r}_0) e^{-ik_x md/2} e^{ik_y md\sqrt{3}/2} e^{-\kappa md\sqrt{3}/2}. \end{aligned} \quad (3)$$

We show in the Appendix that in the braided region,  $\varphi_2(x, y) = \varphi_1^*(-x, y)$  and that the modes have equal magnitudes with  $c_2 = e^{i\vartheta} c_1^*$ , thus we choose the origin such that  $\mathbf{r}_0 = (0, y_0)$  and get

$$\psi(\mathbf{r}_0 + m\mathbf{e}_2) = 2e^{-\kappa md\sqrt{3}/2} e^{-ik_x md/2} \text{Re} \left[ c_1 \varphi_1(\mathbf{r}_0) e^{i(k_y md\sqrt{3}/2 + i\vartheta/2)} \right]. \quad (4)$$

Therefore in the barrier region the PCW mode consists of a decaying envelope modulating a periodic oscillation. When a second waveguide is situated on a zero of this oscillation, the PCWs do not couple and their modes are degenerate. Though the relative phase  $\vartheta$  is known only after computing the single PCW mode, Eq. (4) shows that the serpentine nature of the coupled PCW bands is due to the interference of the two evanescent Bloch modes in the barrier.

We now examine the symmetry of the CWMs. Dossou *et al* [16] showed that the fundamental mode of coupled point defects has the same symmetry as the underlying bulk Bloch mode. We have observed the same behaviour here for CWMs. Two CPCWs separated by  $\ell$  rows have cylinder centers which are a distance  $(\ell + 1)\mathbf{e}_2$  apart. The fundamental mode is a superposition of the two individual PCW modes such that the phase difference between the two PCWs is that of the underlying bulk Bloch mode. Since the underlying bulk PC has two Bloch modes, we combine these as in Eq. (4) and write

$$|\Psi\rangle = |\psi_1\rangle \pm e^{-ik_x(\ell+1)d/2} |\psi_2\rangle \quad (5)$$

where  $|\psi_1\rangle$  is the mode of the single waveguide,  $\psi_2(\mathbf{r}) = \psi_1(\mathbf{r} + (\ell + 1)\mathbf{e}_2)$ , shown in Fig. 5(b), and the sign is given by  $\text{sgn}[\text{Re}(c_1 \varphi_1(\mathbf{r}_0) e^{i(k_y(\ell+1)d\sqrt{3}/2 + i\vartheta/2)})]$ . The effect of the real part of the exponent is to flip the sign of the fundamental mode as  $k_x$  moves along the BZ. A special case occurs when  $k_x d = \pi$ , i.e. at the BZ edge. As shown in the Appendix, the single PCW mode can be written as a real valued function at the BZ-edge and thus we have  $c_1 = c_2$ . Figure 3(c) shows that at  $k_x d = \pi$  there are two dominant evanescent Bloch modes (the third is separated by a reciprocal lattice vector) where  $\text{Re}(k_y) = \pm\pi/(d\sqrt{3})$  along the entire bandgap. Thus Eq. (4) becomes

$$\psi(\mathbf{r}_0 + m\mathbf{e}_2) = 2e^{-\kappa md\sqrt{3}/2} e^{-ik_x md/2} c_1 \varphi_1(\mathbf{r}_0) \cos(m\pi/2). \quad (6)$$

We find the coupling goes to zero for all odd  $m$  causing the degeneracy seen in Fig. 2(c). For even  $m$  the coupling is locally maximized. Using Eq. (5), the modes at the BZ-edge are  $|\Psi\rangle = |\psi_1\rangle \pm i|\psi_2\rangle$ . This is illustrated by the  $H_z$  field densities in Fig. 4(a)–4(d). Here, both modes have fields that are completely imaginary in one PCW, but are real in the other.

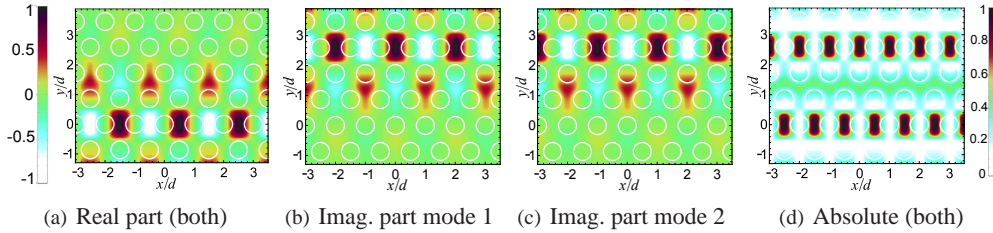


Fig. 4.  $H_z$  fields for two degenerate coupled waveguide modes separated by two rows at  $k_x d = \pi$ . (a) The real part of both modes is identical. (b) The imaginary part of mode 1. (c) Imaginary part of mode 2. (d) Both modes have the same absolute value.

### 3. Formulation of the perturbation theory

To analyse the behaviour of the modes in the braided region rigorously, we now present a perturbation analysis of the coupled PC waveguide modes. Given the mode of a single PC waveguide, this method allows the computation of the coupled waveguide mode frequency splitting relative to the single waveguide mode. The perturbation approximation is derived from a rigorous dispersion equation which is presented in the next two sections.

#### 3.1. Computation of the modes of the unperturbed photonic crystals

We fix the normalized frequency  $d/\lambda$  and the component  $k_x \in \mathbb{R}$  of the wave vector  $\mathbf{k}$ . Let  $k_0 = 2\pi/\lambda$  and  $n_0$  denote respectively the free space wave number and the refractive index of the PC background medium. The infinite two-dimensional PC is modelled as a periodic stack of grating layers [see Fig. 5(a)]. The fields  $H_{z,1}(x, y)$  near the upper interface  $\Pi_1$  and  $H_{z,2}(x, y)$  near the lower interface  $\Pi_2$  of a grating layer can be represented by plane wave expansions [17]:

$$H_{z,s}(x, y) = \sum_{p=-\infty}^{+\infty} \chi_p^{-\frac{1}{2}} \left[ f_{p,s}^- e^{-i\chi_p(y-y_s)} + f_{p,s}^+ e^{i\chi_p(y-y_s)} \right] e^{i\alpha_p(x-x_s)}, \quad \text{for } s = 1, 2, \quad (7)$$

where  $s = 1$  and  $s = 2$  refer respectively to quantities related to the interfaces  $\Pi_1$  and  $\Pi_2$ . The points  $P_1 = (x_1, y_1)$  and  $P_2 = (x_2, y_2)$  are the chosen phase origins [see Fig. 5(a)]. The symbols  $\alpha_p$  and  $\chi_p$  are defined as  $\alpha_p = k_x + 2\pi p/d$  and  $\chi_p = (n_0^2 k_0^2 - \alpha_p^2)^{1/2}$ ,  $\forall p \in \mathbb{Z}$ .

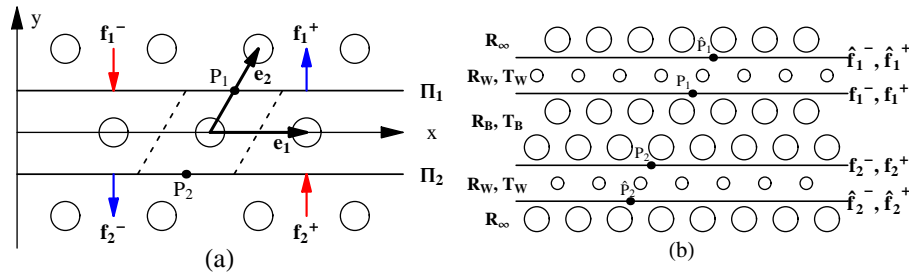


Fig. 5. (a): Geometry of the PC unit cell, defined by the basis vectors  $\mathbf{e}_1$  and  $\mathbf{e}_2$ . Points  $P_1$  and  $P_2$  are the phase origins of the plane wave expansion respectively at the upper ( $\Pi_1$ ) and lower ( $\Pi_2$ ) interfaces of a grating layer. (b): Schematic of a PC with a double waveguide, a composite of 5 elements characterized by their scattering matrices:  $\mathbf{R}_W$ ,  $\mathbf{T}_W$  for the waveguides,  $\mathbf{R}_B$ ,  $\mathbf{T}_B$  for the barrier between the waveguides and  $\mathbf{R}_\infty$  for the semi-infinite PCs.

The transfer matrix  $\mathcal{T}$  relates the fields at upper and lower interfaces of the grating. If we denote by  $\mathbf{f}_1^-$ ,  $\mathbf{f}_1^+$ ,  $\mathbf{f}_2^-$  and  $\mathbf{f}_2^+$  the column vectors whose elements are respectively the plane wave expansion coefficients  $f_{p,1}^-$ ,  $f_{p,1}^+$ ,  $f_{p,2}^-$  and  $f_{p,2}^+$  in Eq. (7), then the Bloch modes are given by the condition

$$\mathcal{T} \begin{bmatrix} \mathbf{f}_1^- \\ \mathbf{f}_1^+ \end{bmatrix} = \mu \begin{bmatrix} \mathbf{f}_1^- \\ \mathbf{f}_1^+ \end{bmatrix} \quad (8)$$

where  $\mu$  is the phase factor  $\mu = e^{-ik \cdot \mathbf{e}_2}$ . Thus the Bloch modes are the eigenvectors of the transfer matrix  $\mathcal{T}$  of a single grating layer;  $\mathcal{T}$  can be diagonalized as  $\mathcal{T} = \mathcal{F} \mathcal{L} \mathcal{F}^{-1}$  where

$$\mathcal{F} = \begin{bmatrix} \mathbf{F}_- & \mathbf{F}'_- \\ \mathbf{F}_+ & \mathbf{F}'_+ \end{bmatrix} \quad \text{and} \quad \mathcal{L} = \begin{bmatrix} \Lambda & \mathbf{0} \\ \mathbf{0} & \Lambda' \end{bmatrix}. \quad (9)$$

In Eq. (9) the columns of  $\mathcal{F}$  represent the eigenvectors which constitute the Bloch modes [17]. The left partition  $\mathbf{F}_-$  and  $\mathbf{F}_+$  contain the downward propagating modes, whereas the right partition contains the upward propagating modes. The matrix  $\mathcal{L}$  is diagonal and comprises the eigenvalues  $\mu$ , partitioned into downward ( $\Lambda$ ) and upward propagating ( $\Lambda'$ ) modes. The grating layer in Fig. 5(a) has up-down symmetry, i.e., it is invariant by the transformation  $(x, y) \mapsto (x, -y)$ , assuming without loss of generality that the coordinate origin is the midpoint between  $P_1$  and  $P_2$ . This transformation changes a downward propagating mode into an upward propagating mode and vice-versa. It also permutes the fields [and their plane wave expansions (7)] at the lower interface and upper interfaces. To obtain the new plane wave expansion, for instance, at the upper interface, we must take into account  $(x - x_2) = (x - x_1) - d/2$ , i.e.,  $P_1$  and  $P_2$  are shifted horizontally by a half period, together with  $(-y - y_2) = -(y - y_1)$ . It follows from these properties that the downward and upward propagating modes can be chosen such that they satisfy the symmetry relations

$$\Lambda' \Lambda = e^{-ik_x d} \mathbf{I}, \quad \begin{bmatrix} \mathbf{F}'_- \\ \mathbf{F}'_+ \end{bmatrix} = \begin{bmatrix} \mathbf{Q}_0 \mathbf{F}_+ \\ \mathbf{Q}_0 \mathbf{F}_- \end{bmatrix} \quad \text{and} \quad \mathbf{Q}_0 = \text{diag} (e^{ip\pi})_{p \in \mathbb{Z}} = \text{diag} ((-1)^p)_{p \in \mathbb{Z}}. \quad (10)$$

### 3.2. Photonic crystal waveguides

To derive a dispersion equation for the double waveguide in Fig. 5(b), we model the structure as a composite of 5 elements: the upper and lower waveguides, a barrier consisting of  $\ell$  periodic PC layers, and upper and lower semi-infinite PCs. Each element is characterised by its reflection and transmission matrices under plane wave incidence. Since the phase origins  $P_1$  and  $P_2$  are shifted horizontally, incidence by downward propagating plane waves (on the upper interface) and by upward propagating plane waves (on the lower interface) have different scattering matrices; primed symbols apply to the matrices of the latter case. Let  $\mathbf{R}_W$ ,  $\mathbf{T}_W$ ,  $\mathbf{R}'_W$  and  $\mathbf{T}'_W$  denote the plane wave scattering matrices of a single waveguide. The scattering matrices of the barrier are denoted  $\mathbf{R}_B$ ,  $\mathbf{T}_B$ ,  $\mathbf{R}'_B$  and  $\mathbf{T}'_B$ . The Fresnel reflection matrices of semi-infinite PCs are represented by  $\mathbf{R}_\infty$  and  $\mathbf{R}'_\infty$ . From Botten *et al.* [17], the scattering matrices of the barrier and the semi-infinite PCs can be computed using the Bloch modes of the unperturbed PCs

$$\mathbf{R}_\infty = \mathbf{F}_+ \mathbf{F}_-^{-1} \quad \text{and} \quad \mathbf{R}'_\infty = \mathbf{F}'_- \mathbf{F}'_+^{-1} \quad (11a)$$

$$\mathbf{R}_B = \mathbf{F}'_+ \left( -\mathbf{R}_{21} + \Lambda'^{-\ell} \mathbf{R}_{21} \Lambda^\ell \right) \left( \mathbf{I} - \mathbf{R}'_{21} \Lambda'^{-\ell} \mathbf{R}_{21} \Lambda^\ell \right)^{-1} \mathbf{F}_-^{-1} \quad (11b)$$

$$\mathbf{T}_B = \mathbf{F}_- \left( \mathbf{I} - \mathbf{R}'_{21} \mathbf{R}_{21} \right) \Lambda^\ell \left( \mathbf{I} - \mathbf{R}'_{21} \Lambda'^{-\ell} \mathbf{R}_{21} \Lambda^\ell \right)^{-1} \mathbf{F}_-^{-1} \quad (11c)$$

$$\mathbf{R}'_B = \mathbf{F}_- \left( -\mathbf{R}'_{21} + \Lambda^\ell \mathbf{R}'_{21} \Lambda'^{-\ell} \right) \left( \mathbf{I} - \mathbf{R}_{21} \Lambda^\ell \mathbf{R}'_{21} \Lambda'^{-\ell} \right)^{-1} \mathbf{F}'_+^{-1} \quad (11d)$$

$$\mathbf{T}'_B = \mathbf{F}'_+ \left( \mathbf{I} - \mathbf{R}_{21} \mathbf{R}'_{21} \right) \Lambda'^{-\ell} \left( \mathbf{I} - \mathbf{R}_{21} \Lambda^\ell \mathbf{R}'_{21} \Lambda'^{-\ell} \right)^{-1} \mathbf{F}'_+^{-1} \quad (11e)$$

with  $\mathbf{R}_{21} = -\mathbf{F}'_+{}^{-1}\mathbf{F}_+$  and  $\mathbf{R}'_{21} = -\mathbf{F}_-{}^{-1}\mathbf{F}'_-$ ;  $\mathbf{R}_{21}$  and  $\mathbf{R}'_{21}$  are the Fresnel reflection matrices for Bloch mode incidence on a semi-infinite homogeneous background material. The scattering matrices  $\mathbf{R}_W$ ,  $\mathbf{T}_W$ ,  $\mathbf{R}'_W$  and  $\mathbf{T}'_W$  can be computed by solving a grating diffraction problem. However these scattering matrices can be obtained analytically if a waveguide is created by removing a row of cylinders: since the waveguide is homogeneous and has the same refractive index as the background,  $\mathbf{R}_W = \mathbf{R}'_W = \mathbf{0}$ ,  $\mathbf{T}_W = \exp(ik_x d/2) \mathbf{Q}_0 \mathbf{P}$  and  $\mathbf{T}'_W = \exp(-ik_x d/2) \mathbf{Q}_0 \mathbf{P}$  with  $\mathbf{P} = \text{diag}(\exp(i\chi_p h))$  and  $h = d\sqrt{3}/2$ . In the general case of waveguide gratings,  $\mathbf{R}_W \neq \mathbf{0}$  and, at the upper waveguide, we have the plane wave scattering relations

$$\begin{cases} \hat{\mathbf{f}}_1^+ = \mathbf{R}_W \hat{\mathbf{f}}_1^- + \mathbf{T}'_W \mathbf{f}_1^+ \\ \hat{\mathbf{f}}_1^- = \mathbf{T}_W \hat{\mathbf{f}}_1^- + \mathbf{R}'_W \mathbf{f}_1^+ \\ \hat{\mathbf{f}}_1^- = \mathbf{R}'_\infty \hat{\mathbf{f}}_1^+ \end{cases} \implies \begin{cases} \hat{\mathbf{f}}_1^+ = (\mathbf{I} - \mathbf{R}_W \mathbf{R}'_\infty)^{-1} \mathbf{T}'_W \mathbf{f}_1^+ \\ \hat{\mathbf{f}}_1^- = \mathbf{R}'_\infty (\mathbf{I} - \mathbf{R}_W \mathbf{R}'_\infty)^{-1} \mathbf{T}'_W \mathbf{f}_1^+ \\ \hat{\mathbf{f}}_1^- = (\mathbf{R}'_W + \mathbf{T}_W \mathbf{R}'_\infty (\mathbf{I} - \mathbf{R}_W \mathbf{R}'_\infty)^{-1} \mathbf{T}'_W) \mathbf{f}_1^+ \end{cases} \quad (12)$$

Similarly for the lower waveguide we obtain

$$\mathbf{f}_2^+ = (\mathbf{R}_W + \mathbf{T}'_W \mathbf{R}_\infty (\mathbf{I} - \mathbf{R}'_W \mathbf{R}_\infty)^{-1} \mathbf{T}_W) \mathbf{f}_2^-. \quad (13)$$

We have the relations across the barrier between the two waveguides

$$\mathbf{f}_1^+ = \mathbf{R}_B \mathbf{f}_1^- + \mathbf{T}'_B \mathbf{f}_2^+ \quad \text{and} \quad \mathbf{f}_2^- = \mathbf{T}_B \mathbf{f}_1^- + \mathbf{R}'_B \mathbf{f}_2^+. \quad (14)$$

We now use the symmetry relations (10) to halve the size of the eigenproblem and so get some insight about the symmetry of the modes. It follows from Eq. (10) that the scattering matrices in Eqs (11a)–(11e) and Eq. (13) satisfy the symmetry properties (note that  $\mathbf{Q}_0^{-1} = \mathbf{Q}_0$ )

$$\mathbf{R}'_B = \mathbf{Q}_0 \mathbf{R}_B \mathbf{Q}_0, \quad \mathbf{T}'_B = e^{i\ell k_x d} \mathbf{Q}_0 \mathbf{T}_B \mathbf{Q}_0 \quad \text{and} \quad \mathbf{R}'_{21} = \mathbf{R}_{21}. \quad (15)$$

Next, we translate horizontally the bottom phase origin  $P_2$  of the barrier by  $\Delta x = \ell d/2$ ; the new phase origin is aligned vertically with the top phase origin  $P_1$  which is useful for analyzing the field symmetry. With the new phase origin, the expression for the vector of plane wave coefficients  $\mathbf{f}_2$  is

$$\tilde{\mathbf{f}}_2 = \text{diag}\left(e^{\frac{i\alpha_p \ell d}{2}}\right) \mathbf{f}_2 = e^{\frac{ik_x \ell d}{2}} \mathbf{Q}_0^\ell \mathbf{f}_2. \quad (16)$$

Substituting the relations (15) into Eq. (14), together with Eq. (16) gives

$$\left(\mathbf{f}_1^+ \pm \mathbf{Q}_0^{\ell+1} \tilde{\mathbf{f}}_2^-\right) = \left(\mathbf{R}_B \pm e^{\frac{ik_x \ell d}{2}} \mathbf{Q}_0 \mathbf{T}_B\right) \left(\mathbf{f}_1^- \pm \mathbf{Q}_0^{\ell+1} \tilde{\mathbf{f}}_2^+\right) \quad (17)$$

with both relations holding simultaneously. A similar treatment for the Fresnel-type equations (13) and its counterpart in Eq. (12), together with the symmetry relations

$$\mathbf{R}'_\infty = \mathbf{Q}_0 \mathbf{R}_\infty \mathbf{Q}_0, \quad (18)$$

$$\mathbf{R}_W + \mathbf{T}'_W \mathbf{R}_\infty (\mathbf{I} - \mathbf{R}'_W \mathbf{R}_\infty)^{-1} \mathbf{T}_W = \mathbf{Q}_0 \left(\mathbf{R}'_W + \mathbf{T}_W \mathbf{R}'_\infty (\mathbf{I} - \mathbf{R}_W \mathbf{R}'_\infty)^{-1} \mathbf{T}'_W\right) \mathbf{Q}_0. \quad (19)$$

yield

$$\mathbf{f}_1^- = \bar{\mathbf{R}} \mathbf{f}_1^+ \quad \text{and} \quad \mathbf{Q}_0^{\ell+1} \tilde{\mathbf{f}}_2^+ = \bar{\mathbf{R}} \mathbf{Q}_0^{\ell+1} \tilde{\mathbf{f}}_2^-. \quad (20)$$

Hence

$$\left(\mathbf{f}_1^- \pm \mathbf{Q}_0^{\ell+1} \tilde{\mathbf{f}}_2^+\right) = \bar{\mathbf{R}} \left(\mathbf{f}_1^+ \pm \mathbf{Q}_0^{\ell+1} \tilde{\mathbf{f}}_2^-\right) \quad (21)$$



where

$$\bar{\mathbf{R}} = \mathbf{R}'_W + \mathbf{T}_W \mathbf{R}'_\infty (\mathbf{I} - \mathbf{R}_W \mathbf{R}'_\infty)^{-1} \mathbf{T}'_W. \quad (22)$$

Substituting expression (21) into Eq. (17) leads to

$$\mathbf{A}(\sigma) \left( \mathbf{f}_1^+ + \sigma \mathbf{Q}_0^{\ell+1} \tilde{\mathbf{f}}_2^+ \right) = \mathbf{0}, \quad \text{with} \quad \mathbf{A}(\sigma) = \mathbf{I} - \left( \mathbf{R}_B + \sigma e^{\frac{ik_x \ell d}{2}} \mathbf{Q}_0 \mathbf{T}_B \right) \bar{\mathbf{R}} \quad (23)$$

where  $\sigma = 1$  gives one equation and  $\sigma = -1$  gives the other, both of which are simultaneously true. For a pair of coupled waveguide modes,  $\mathbf{f}_1^+$  or  $\tilde{\mathbf{f}}_2^+$  are not zero, so if  $\mathbf{A}(\sigma)$  is singular then, in general,  $\mathbf{A}(-\sigma)$  is not. Thus the dispersion equation is given by  $\det \mathbf{A}(\sigma) = 0$  while the mode symmetry follows from  $\mathbf{f}_1^+ - \sigma \mathbf{Q}_0^{\ell+1} \tilde{\mathbf{f}}_2^+ = \mathbf{0}$ . In particular when  $\ell$  is odd we have  $\mathbf{Q}_0^{\ell+1} = \mathbf{I}$  so that  $\mathbf{f}_1^+ = \sigma \tilde{\mathbf{f}}_2^+$  and, from Eq. (20),  $\mathbf{f}_1^- = \sigma \tilde{\mathbf{f}}_2^+$ , i.e., the waveguide mode has even symmetry when  $\sigma = 1$  and odd symmetry when  $\sigma = -1$ . In practice, the nonlinear eigenvalue problems can be solved by searching for the roots of the determinant of the matrix  $\mathbf{A}(\sigma)$ .

As the thickness parameter  $\ell$  increases,  $\mathbf{R}_B$  tends to  $\mathbf{R}_\infty$  while  $\mathbf{T}_B$  tends to zero since the bulk PC is in a band gap. We obtain the single waveguide dispersion equation as  $\ell \rightarrow \infty$

$$\mathbf{A}_0 \mathbf{f}_1^+ = \mathbf{0} \quad \text{with} \quad \mathbf{A}_0 = \mathbf{I} - \mathbf{R}_\infty \bar{\mathbf{R}}. \quad (24)$$

### 3.3. Perturbation theory

We assume that the propagation constant  $k_x$  is fixed while the normalized frequency  $\nu = d/\lambda$  is unknown. The dispersion equation (23) for the double waveguide problem is equivalent to finding a frequency  $\nu$  and a mode  $\mathbf{x}$  such that  $\mathbf{A}(\sigma, \nu) \mathbf{x} = \mathbf{0}$ . Similarly, for a single waveguide, we write the dispersion equation as  $\mathbf{A}_0(\nu_0) \mathbf{x}_0 = \mathbf{0}$ . To find a solution through a perturbation analysis, we consider the problem (23) as a perturbation to Eq. (24) and introduce the notation

$$\nu = \nu_0 + \delta\nu, \quad \mathbf{x} = \mathbf{x}_0 + \delta\mathbf{x} \quad \text{and} \quad \mathbf{A}(\sigma, \nu) = \mathbf{A}_0(\nu_0 + \delta\nu) + \delta\mathbf{A}(\sigma, \nu_0 + \delta\nu). \quad (25)$$

The term  $\delta\mathbf{A}$ , which accounts for the perturbation due to the finite width of the barrier between the waveguides, is defined below in Eq. (33). The equation  $\mathbf{A}(\sigma, \nu) \mathbf{x} = \mathbf{0}$  is thus that for

$$\left( \mathbf{A}_0(\nu_0 + \delta\nu) + \delta\mathbf{A}(\sigma, \nu_0 + \delta\nu) \right) (\mathbf{x}_0 + \delta\mathbf{x}) = \mathbf{0}. \quad (26)$$

As a first order analysis, we can derive the leading order equation

$$\left( \mathbf{A}_0(\nu_0) + \frac{\partial \mathbf{A}_0}{\partial \nu} \delta\nu + \delta\mathbf{A}(\sigma, \nu_0) \right) (\mathbf{x}_0 + \delta\mathbf{x}) = \mathbf{0}. \quad (27)$$

The size of the matrix  $\mathbf{A}_0 = \mathbf{I} - \mathbf{R}_\infty \bar{\mathbf{R}}$  is the number of plane wave orders included in our calculations. When the plane wave orders are truncated to just the propagating plane wave orders, then the matrices  $\mathbf{R}_\infty$  and  $\bar{\mathbf{R}}$  are unitary when the background PC is in a bandgap (as a consequence,  $\mathbf{R}_\infty \bar{\mathbf{R}}$  is also unitary). For the PCs considered here, there are either one or two propagating plane wave orders. The most interesting cases, corresponding to the braided region, have two propagating plane wave orders. Then the unitary matrix  $\mathbf{R}_\infty \bar{\mathbf{R}}$  has two orthogonal eigenvectors  $\mathbf{x}_0^{(1)}$  and  $\mathbf{x}_0^{(2)}$  associated respectively with eigenvalues  $\gamma_1$  and  $\gamma_2$ . The single waveguide equation  $\mathbf{A}_0 \mathbf{x} = (\mathbf{I} - \mathbf{R}_\infty \bar{\mathbf{R}}) \mathbf{x} = \mathbf{0}$  has a solution if 1 is an eigenvalue of the matrix  $\mathbf{R}_\infty \bar{\mathbf{R}}$ . Let assume, for instance, that the eigenvector  $\mathbf{x}_0^{(1)}$  is associated with the eigenvalue  $\gamma_1 = 1$  and construct the solution of the double waveguide as the perturbation

$$\mathbf{x} = \mathbf{x}_0 + \delta\mathbf{x} = \mathbf{x}_0^{(1)} + c^{(1)} \mathbf{x}_0^{(1)} + c^{(2)} \mathbf{x}_0^{(2)} \quad \text{with} \quad |c^{(1)}| \ll 1 \quad \text{and} \quad |c^{(2)}| \ll 1. \quad (28)$$

By substituting this expression in Eq. (27) and using the fact that  $\mathbf{A}_0(v_0)\mathbf{x}_0^{(1)} = \mathbf{0}$ , we are led to the first order perturbation equation

$$\delta v \frac{\partial \mathbf{A}_0}{\partial v} \mathbf{x}_0^{(1)} = -\delta \mathbf{A}(\sigma, v_0) \mathbf{x}_0^{(1)} - c^{(2)} \mathbf{A}_0(v_0) \mathbf{x}_0^{(2)}. \quad (29)$$

and by taking the inner product with  $\mathbf{x}_0^{(1)}$ , we find

$$\delta v = -\frac{\mathbf{x}_0^{(1)H} \delta \mathbf{A}(\sigma, v_0) \mathbf{x}_0^{(1)}}{\mathbf{x}_0^{(1)H} \frac{\partial \mathbf{A}_0}{\partial v} \mathbf{x}_0^{(1)}} \quad (30)$$

since  $\mathbf{x}_0^{(1)H} (\mathbf{A}_0(v_0) \mathbf{x}_0^{(2)}) = (1 - \gamma_2) \mathbf{x}_0^{(1)H} \mathbf{x}_0^{(2)} = 0$ . The superscript  $H$  denotes the Hermitian transpose, i.e., the conjugate transpose. A matrix norm is used in the analysis below and any type of norm can be considered since, in a finite dimensional space, all matrix norms are equivalent. From Eqs. (11a)–(11c) and (15), we can derive the leading order estimates with respect to the small parameter  $\|\mathbf{\Lambda}^\ell\|$

$$\mathbf{R}_B = \mathbf{R}_\infty + O(\|\mathbf{\Lambda}^\ell\|^2) \quad (31)$$

$$\mathbf{T}_B = \mathbf{F}_- (\mathbf{I} - \mathbf{R}_{21}^2) \mathbf{\Lambda}^\ell \mathbf{F}_-^{-1} + O(\|\mathbf{\Lambda}^\ell\|^2) = (\mathbf{I} - (\mathbf{Q}_0 \mathbf{R}_\infty)^2) \mathbf{F}_- \mathbf{\Lambda}^\ell \mathbf{F}_-^{-1} + O(\|\mathbf{\Lambda}^\ell\|^2) \quad (32)$$

and it follows that

$$\delta \mathbf{A}(\sigma, v) = \mathbf{A}(\sigma, v) - \mathbf{A}_0(v) = -\sigma e^{\frac{ik_x \ell d}{2}} \mathbf{Q}_0 (\mathbf{I} - (\mathbf{Q}_0 \mathbf{R}_\infty)^2) \mathbf{F}_- \mathbf{\Lambda}^\ell \mathbf{F}_-^{-1} \overline{\mathbf{R}} + O(\|\mathbf{\Lambda}^\ell\|^2) \quad (33)$$

so that, to leading order, the numerator  $\mathbf{x}_0^{(1)H} \delta \mathbf{A}(\sigma, v_0) \mathbf{x}_0^{(1)}$  is given by

$$\mathbf{x}_0^{(1)H} \delta \mathbf{A}(\sigma, v_0) \mathbf{x}_0^{(1)} = -\sigma \mathbf{x}_0^{(1)H} \mathbf{Q}_0 (\mathbf{I} - (\mathbf{Q}_0 \mathbf{R}_\infty)^2) \mathbf{F}_- \left( e^{\frac{ik_x d}{2}} \mathbf{\Lambda} \right)^\ell \mathbf{F}_-^{-1} \overline{\mathbf{R}} \mathbf{x}_0^{(1)} \quad (34)$$

or

$$\mathbf{x}_0^{(1)H} \delta \mathbf{A}(\sigma, v_0) \mathbf{x}_0^{(1)} = -\sigma \mathbf{x}_0^{(1)H} \mathbf{Q}_0 (\mathbf{I} - (\mathbf{Q}_0 \mathbf{R}_\infty)^2) \mathbf{F}_- \left( e^{\frac{ik_x d}{2}} \mathbf{\Lambda} \right)^\ell \mathbf{F}_-^{-1} \mathbf{R}_\infty^{-1} \mathbf{x}_0^{(1)} \quad (35)$$

since, from Eq. (24),  $\mathbf{R}_\infty \overline{\mathbf{R}} \mathbf{x}_0^{(1)} = \mathbf{x}_0^{(1)}$ . The denominator term  $\mathbf{x}_0^{(1)H} \frac{\partial \mathbf{A}_0}{\partial v} \mathbf{x}_0^{(1)}$  is also derived from Eq. (24)

$$\mathbf{x}_0^{(1)H} \frac{\partial \mathbf{A}_0}{\partial v} \mathbf{x}_0^{(1)} = -\mathbf{x}_0^{(1)H} \frac{\partial \left( \mathbf{R}_\infty(v) \overline{\mathbf{R}}(v) \right)}{\partial v} \mathbf{x}_0^{(1)}. \quad (36)$$

From unitarity and mode orthogonality  $\mathbf{R}^H \mathbf{T}' + \mathbf{T}^H \mathbf{R}' = \mathbf{0}$ , for propagating plane orders only (see Ref. [18, Eq. (24b)]), it follows that the matrix  $\exp(ik_x \ell d/2) \mathbf{Q}_0 \mathbf{T} \mathbf{R}^{-1}$  is skew-hermitian, and as a consequence its leading term is also skew-hermitian. Thus  $\mathbf{x}_0^{(1)H} \delta \mathbf{A}(v_0) \mathbf{x}_0^{(1)}$  is a pure imaginary number. The denominator  $\mathbf{x}_0^{(1)H} \frac{\partial \mathbf{A}_0}{\partial v} \mathbf{x}_0^{(1)}$  in Eq. (36) is also pure imaginary at  $v = v_0$ . We prove this by using  $\mathbf{R}_\infty \overline{\mathbf{R}} \mathbf{x}_0^{(1)} = \left( \mathbf{R}_\infty \overline{\mathbf{R}} \right)^H \mathbf{x}_0^{(1)} = \mathbf{x}_0^{(1)}$  and the fact that the derivative of a parameterized family of unitary matrices  $\mathbf{U}(v)$  is skew-hermitian at  $v = v_0$  if  $\mathbf{U}(v_0) = \mathbf{I}$  since, from  $\mathbf{U}(v) \mathbf{U}^H(v) = \mathbf{I}$ , we have  $\mathbf{0} = \left( \mathbf{U}(v) \mathbf{U}^H(v) \right)' = \mathbf{U}'(v) \mathbf{U}^H(v) + \mathbf{U}(v) \mathbf{U}'^H(v)$  and in particular  $\mathbf{U}'(v_0) + \mathbf{U}'^H(v_0) = \mathbf{0}$ . The parameterized family  $\mathbf{U}(v) = \left( \mathbf{R}_\infty(v_0) \mathbf{P}(v_0) \right)^H \mathbf{R}_\infty(v) \mathbf{P}(v)$  satisfies such a property. Since the denominator does not depend on the length  $\ell$ , to study the

impact of the barrier thickness  $\ell$  on the frequency shift  $\delta v$  in Eq. (30), we just have to analyze the numerator (35). Since  $\mathbf{R}_\infty$  is unitary, we can show that Eq. (35) can be written as

$$\mathbf{x}_0^{(1)H} \delta \mathbf{A}(\sigma, v_0) \mathbf{x}_0^{(1)} = \sigma \mathbf{x}_0^{(1)H} (\mathbf{Q}_0 \mathbf{R}_\infty^H \mathbf{Q}_0 - \mathbf{R}_\infty) \mathbf{Q}_0 \mathbf{F}_+ \left( e^{\frac{ik_x d}{2}} \boldsymbol{\Lambda} \right)^\ell \mathbf{F}_+^{-1} \mathbf{x}_0^{(1)} \quad (37)$$

and when only one propagating plane wave order exists, Eq. (30) simplifies to a scalar problem:

$$\delta v = \sigma \frac{\text{Im}(\mathbf{R}_\infty)}{\frac{\partial(\mathbf{R}_\infty(v) \overline{\mathbf{R}}(v))}{\partial v}} \left( e^{\frac{ik_x d}{2}} \mu_1 \right)^\ell \quad (38)$$

which is a generalisation of Eq. (20) in Ref. [19].

In the cases where two propagating plane wave orders are considered, there are two evanescent modes with Bloch factors  $\mu_1$  and  $\mu_2$ , and Eq. (37) takes the form

$$\mathbf{x}_0^{(1)H} \delta \mathbf{A}(v_0) \mathbf{x}_0^{(1)} = \sigma \left( a_1 \left( e^{\frac{ik_x d}{2}} \mu_1 \right)^\ell + a_2 \left( e^{\frac{ik_x d}{2}} \mu_2 \right)^\ell \right). \quad (39)$$

If one of the evanescent Bloch modes is dominant, i.e., for instance,  $|\mu_1| > |\mu_2|$ , when  $\ell$  is large enough  $|\mu_2|^\ell$  becomes negligible with respect to  $|\mu_1|^\ell$  and we get

$$\delta v \approx \sigma a_1 \left( e^{\frac{ik_x d}{2}} \mu_1 \right)^\ell. \quad (40)$$

When  $\mu_1$  is associated with a dominant evanescent mode (as in Eqs (38) and (40)) the quantity  $(\exp(ik_x d/2) \mu_1)$  must be real. Otherwise, as shown below, we can find  $\mu_2 \neq \mu_1$  such that  $|\mu_2| = |\mu_1|$ . If  $(\exp(ik_x d/2) \mu)$  is real and negative, we get an oscillatory dependence since the sign of  $\delta v$  depends on the parity of  $\ell$ .

Indeed when  $(\exp(ik_x d/2) \mu_1)$  has a nonzero imaginary part, if  $\varphi_1(x, y)$  is an associated Bloch mode, from the invariance of the PC lattice with the geometric transformation  $(x, y) \mapsto (-x, y)$ , it follows that for lossless PC,  $\varphi_2 = \varphi_1^*(-x, y)$  is a Bloch mode associated with  $k_x$  and

$$e^{\frac{ik_x d}{2}} \mu_2 = \left( e^{\frac{ik_x d}{2}} \mu_1 \right)^* \neq e^{\frac{ik_x d}{2}} \mu_1. \quad (41)$$

This also means that  $|\mu_1| = |\mu_2|$ , i.e.,  $\varphi_1(x, y)$  and  $\varphi_2(x, y)$  form a pair of linearly independent dominant evanescent Bloch modes. If  $\mathbf{f}_1^-$  and  $\mathbf{f}_1^+$  are vectors of plane wave components of the mode  $\varphi_1(x, y)$  in the plane wave expansion (7), then  $\varphi_2 = \varphi_1^*(-x, y)$  has as components  $\mathbf{f}_2^- = \mathbf{Q}_0 \mathbf{f}_1^{+*}$  and  $\mathbf{f}_2^+ = \mathbf{Q}_0 \mathbf{f}_1^{-*}$ ; matrix  $\mathbf{Q}$  accounts for the fact that the transformation  $(x, y) \mapsto (-x, y)$  shifts the phase origins  $x_0 = d/4$  and  $x'_0 = -d/4$ . Furthermore, when  $(\exp(ik_x d/2) \mu_1)$  and  $(\exp(ik_x d/2) \mu_2)$  form a conjugate pair, to satisfy the requirement that  $\mathbf{x}_0^{(1)H} \delta \mathbf{A}(v_0) \mathbf{x}_0^{(1)}$  be purely imaginary, it is sufficient that the prefactors  $a_1$  and  $a_2$  in Eq. (39) satisfy  $a_2 = -a_1^*$ . Varying  $\ell$  shows that this condition is also necessary. Thus for a pair of dominant evanescent modes, Eq. (39) becomes

$$\begin{aligned} \mathbf{x}_0^{(1)H} \delta \mathbf{A}(v_0) \mathbf{x}_0^{(1)} &= \sigma \left( a_1 \left( e^{\frac{ik_x d}{2}} \mu_1 \right)^\ell - a_1^* \left( e^{-\frac{ik_x d}{2}} \mu_1^* \right)^\ell \right) \\ &= 2 \sigma i |a_1| |\mu_1|^\ell \sin \left( \left( \arg(\mu_1) + \frac{k_x d}{2} \right) \ell + \arg(a_1) \right) \end{aligned} \quad (42)$$

which shows that  $\mathbf{x}_0^{(1)H} \delta \mathbf{A}(v_0) \mathbf{x}_0^{(1)} / |\mu_1|^\ell$  is periodic with respect to  $\ell$ ; in particular for some values of  $\ell$   $\mathbf{x}_0^{(1)H} \delta \mathbf{A}(v_0) \mathbf{x}_0^{(1)} = 0$ , i.e.,  $\delta v = 0$ , although this root is physically meaningful only

Table 1. Crossing points  $(k_x d, d/\lambda)$  of the even and odd CWM dispersion curves in Fig. 1, according to the dispersion results in Fig. 1 (columns “converged results”) and the roots of  $\delta v(k_x, d/\lambda, \ell)$  (columns “perturbation theory”)

Crossing points for $\ell = 4$		Crossing points for $\ell = 5$	
Converged results	Perturbation theory	Converged results	Perturbation theory
(2.0789, 0.3174)	(2.0971, 0.3155)	(2.0531, 0.3176)	(2.0727, 0.3158)
(2.5392, 0.3085)	(2.5428, 0.3073)	(2.3934, 0.3113)	(2.3992, 0.3101)
(2.5492, 0.2956)	(2.5500, 0.2950)	(2.4107, 0.2985)	(2.4121, 0.2979)
$(\pi, 0.2905)$	$(\pi, 0.2898)$	(2.8900, 0.3037)	(2.891, 0.3027)
$(\pi, 0.3028)$	$(\pi, 0.3016)$	(2.8985, 0.2913)	(2.8988, 0.2907)

when  $\ell$  is an integer; if that is the case we have a crossing between the even ( $\sigma = 1$ ) and odd ( $\sigma = -1$ ) dispersion curves of the double waveguides.

Figure 6 shows the root  $\ell$  of  $\delta v$  versus  $k_x d \in [0, \pi]$  when  $(k_x, v_0)$  varies along the dispersion curve of a single waveguide; the crossing points correspond to integer values of the root  $\ell$ . The results in Table 1 show that the first order perturbation theory agrees well with full numerical calculations. The perturbation theory is not accurate near  $k_x d = 1.8555$  where the dispersion relation of a single waveguide is degenerate. For the PCs studied here, such degeneracy occurs outside the braided region so that the perturbation theory is valid inside this region.

For  $k_x d = \pi$ , all even values of  $\ell > 0$  are a root. Our theory explains this property. Since  $k_x d = \pm\pi$  are equivalent wave vector components (same quasi-periodicity with respect to  $\mathbf{e}_1$ ), in addition to  $\varphi_2 = \varphi_1^*(-x, y)$ ,  $\tilde{\varphi}_2 = \varphi_1^*(x, y)$  is also a permissible Bloch mode and since  $\exp(i\pi d/2) = i$ , it follows that  $\{i\mu_1, i\mu_2\} = \{i\mu_1, i\mu_2\}^* = \{-i\mu_1^*, -i\mu_2^*\}$ ; from the assumption that  $i\mu_1$  and  $i\mu_2$  form a conjugate pair, this implies that  $\mu_1 = -\mu_1^*$ , i.e.,  $\mu_1$  is real and  $\mu_2 = -\mu_1$ . Here Eq. (42) is imaginary if  $a_1$  is real. Thus when  $k_x d = \pi$ , Eq. (42) becomes

$$\mathbf{x}_0^{(1)H} \delta \mathbf{A}(v_0) \mathbf{x}_0^{(1)} = \sigma a_1 \left( (i\mu_1)^\ell - (-i\mu_1)^\ell \right) = 2\sigma i a_1 |\mu_1|^\ell \sin\left(\frac{\pi\ell}{2}\right) \quad (43)$$

so that  $\mathbf{x}_0^{(1)H} \delta \mathbf{A}(v_0) \mathbf{x}_0^{(1)} = 0$  when  $\ell$  is even.

#### 4. Discussion and conclusion

We have given a detailed description of coupling of hexagonal lattice PCW modes, showing that their dispersion curves intertwine due to the beating of two equally dominant evanescent Bloch modes in the barrier regions. This work highlights that there is a hierarchy in the understanding of coupled waveguides. In the simplest case involving two conventional waveguides the fundamental mode is always even and the second mode is odd. In the tight-binding limit these modes can be understood as even and odd superpositions of the modes of the individual waveguides. In square lattices, the modes are similar, but the fundamental mode can be odd and the second mode can be even. In the hexagonal lattices we have considered here the coupled modes can be considered complex superpositions of the modes of the individual waveguides, with coefficients which depend on the wavenumber, leading to the braiding effect. While the rigorous perturbation theory from Section 3 explains the observed behaviour very well (see Table 1), considerable insight may be obtained from intuitive description using the complex bands of the barrier region in Section 2.

Though all results described here were obtained for one particular structure, in which only the parameter  $\ell$ , defining the thickness of the barrier separating the waveguide, was varied, the behaviour is generic and applies to coupled waveguides in any type of hexagonal lattice. Sim-

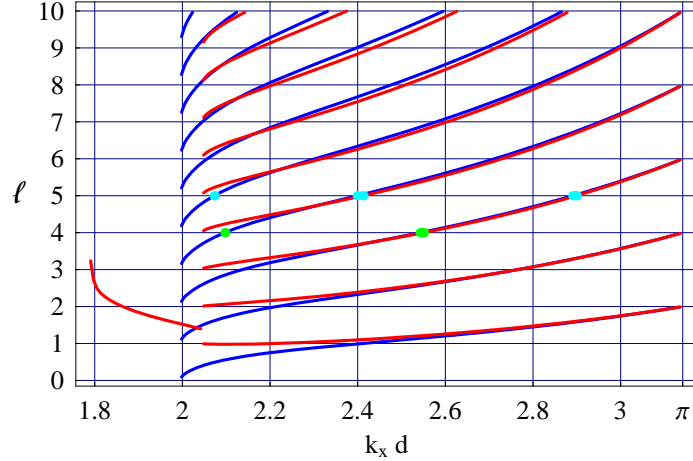


Fig. 6. Roots  $\ell$  of the correction term  $\delta v(k_x, d/\lambda, \ell)$  when  $(k_x d, d/\lambda)$  varies along the dispersion curve of a single waveguide (purple dashed curve in Fig. 1). The roots occurring at  $\ell = 4$  and  $\ell = 5$  are indicated by green and cyan dots respectively (see Table 1 for their coordinates). The blue and red curves correspond, respectively, to the upper and lower frequency modes in the braided region in Fig. 1. The former enters the braided region at  $k_x d = 1.998$ , the latter at  $k_x d = 2.048$ .

ilarly, though the treatment here approximates the PCs as being two-dimensional, our results are generic and apply equally well to slab geometries.

Finally, the braiding leads to complicated dispersion relations, which may have implications for the study of slow light or for the creation of geometry induced, frequency selective index media. In practice the braiding may be somewhat difficult to observe since increasing the spacing between the waveguides, increases the number of intersection points, but decreases the amplitude of the oscillations.

## A. Appendix

In this Appendix, we give detailed justifications of the modal properties discussed in Section 2.

### A.1. Dominant evanescent modes

We assume that the waveguide propagation constant  $k_x \in \mathbb{R}$  and the normalized frequency  $d/\lambda$  are fixed. We consider that we have a directional band gap at  $d/\lambda$  and  $k_x$ . We denote the PC Bloch modes  $\varphi_n(x, y)$  associated with wave vectors of the form  $\mathbf{k}_n = [k_x, k_y] = [k_x, \beta_n + i\kappa_n]$  with  $\beta_n, \kappa_n \in \mathbb{R}$ . Let  $\mathbf{e}_1 = [d, 0]$  and  $\mathbf{e}_2 = [d/2, d\sqrt{3}/2]$  be the lattice vectors of the hexagonal lattice. As discussed in Section 3.1, for fixed values of  $d/\lambda$  and  $k_x$ , the mode  $\varphi_n(x, y)$  can be obtained by solving an eigenproblem where the Bloch factor

$$\mu_n = e^{-i\mathbf{k} \cdot \mathbf{e}_2} = e^{-ik_x d/2} e^{-i\beta_n d\sqrt{3}/2} e^{\kappa_n d\sqrt{3}/2} \quad (44)$$

is the unknown eigenvalue. The cases  $|\mu_n| = 1$  and  $|\mu_n| \neq 1$  correspond respectively to propagating and evanescent Bloch modes. From the band gap assumption, we only have evanescent modes which are classified according to their direction of decay. When  $|\mu_n| < 1$ , the evanescent mode is downward decaying and is denoted  $\varphi_n^-(x, y)$  with the associated eigenvalue  $|\mu_n^-|$ . Similarly,  $\varphi_n^+(x, y)$  represents an upward decaying mode associated with eigenvalue  $|\mu_n^+|$ . The waveguide is modeled as a diffraction grating of thickness  $h = d\sqrt{3}/2$  occupying the domain

$\{(x, y) \mid -h/2 < y < h/2\}$  and surrounded by two semi-infinite PC regions. Let  $\Psi(x, y)$  represent a waveguide mode associated with the waveguide propagation constant  $k_x$  and the normalized frequency  $d/\lambda$ . Following grating diffraction theory, we represent the field  $\Psi(x, y)$  in each semi-infinite as modal expansion of bounded states as

$$\Psi(x, y) = \begin{cases} \sum_{n=1}^{\infty} c_n^+ \varphi_n^+(x, y), & \text{if } y > h/2 \\ \sum_{n=1}^{\infty} c_n^- \varphi_n^-(x, y), & \text{if } y < -h/2 \end{cases} \quad (45)$$

We number the evanescent modes such that  $1 > |\mu_1^-| \geq |\mu_2^-| \geq |\mu_3^-| \geq \dots$  and  $1 < |\mu_1^+| \leq |\mu_2^+| \leq |\mu_3^+| \leq \dots$ , i.e., they are numbered from the least evanescent to the most evanescent. If  $|\mu_1^-| > |\mu_2^-|$  and  $|\mu_1^+| > |\mu_2^+|$ , the contribution from the evanescent modes  $\varphi_1^-(x, y)$  and  $\varphi_1^+(x, y)$  dominate the series in Eq. (45) for large values of  $|y|$  so that the waveguide field  $|\Psi(x, y)|$  decays by a factor  $|\mu_1^-| = |\mu_1^+|$  across each row of PC cylinders [as in Fig. 3(a)].

There are two dominant evanescent modes if  $|\mu_1^-| = |\mu_2^-| > |\mu_3^-|$  and  $|\mu_1^+| = |\mu_2^+| < |\mu_3^+|$ . As we now show, for lossless PCs, a pair of dominant evanescent modes occurs when  $(\beta_1 d \sqrt{3}/2)$  is not a multiple of  $\pi$ . The hexagonal lattice is invariant by the geometric transformation  $T : (x, y) \mapsto (-x, y)$ , since  $T \mathbf{e}_1 = -\mathbf{e}_1$  and  $T \mathbf{e}_2 = \mathbf{e}_2 - \mathbf{e}_1$  are both lattice vectors. It follows that if  $\varphi_1(x, y)$  is a Bloch mode associated with a wave vector  $\mathbf{k} = [k_x, \beta_1 + i \kappa_1]$ , then, for a lossless PC,  $\varphi_1^*(x, y)$  is also a Bloch mode associated  $\mathbf{k} = [-k_x, -\beta_1 + i \kappa_1]$  thus, because of the symmetry,  $\varphi_1^*(-x, y)$  is a Bloch mode which is associated with a permissible wave vector:  $\mathbf{k} = [k_x, -\beta_1 + i \kappa_1]$ . If  $(\beta_1 d \sqrt{3}/2)$  is not a multiple of  $\pi$ , we can derive from the definition (44) that  $\varphi_1(x, y)$  and  $\varphi_1^*(-x, y)$  have the same decay rate  $\kappa$  but different phase factors; thus we can take  $\varphi_2$  as  $\varphi_2 = \varphi_1^*(-x, y)$  and conclude that both  $\varphi_1$  and  $\varphi_2$  are dominant modes.

For a pair of dominant evanescent modes  $\varphi_1$  and  $\varphi_2$  such that  $(\beta_1 d \sqrt{3}/2)$  is not a multiple of  $\pi$ , we can assume, without loss of generality, that  $\varphi_2 = \varphi_1^*(-x, y)$ . As shown below, we can then derive that the coefficients  $c_1$  and  $c_2$  in the series (45) satisfy  $|c_1| = |c_2|$  (if  $\Psi(x, y)$  is non-degenerate). Thus  $\beta_2 = -\beta_1$  and  $|c_1| = |c_2|$  generate a beating between the two evanescent Bloch modes that leads to a field pattern consisting of a decaying envelope modulating a periodic oscillation in Figs. 2(b) and 2(c). We now show that  $|c_1| = |c_2|$ . The field  $\Psi^*(-x, y)$  is also a waveguide mode associated to  $k_x$  and  $d/\lambda$ ; thus if the waveguide mode  $\Psi(x, y)$  is non-degenerate then there exist  $\gamma \in \mathbb{C}$  such that  $|\gamma| = 1$  and  $\Psi^*(-x, y) = \gamma \Psi(x, y)$ . Since  $\varphi_2 = \varphi_1^*(-x, y)$ , the first terms of the modal expansion of  $\Psi^*(-x, y)$  are  $\Psi^*(-x, y) = c_1^* \varphi_2 + c_2^* \varphi_1 + \dots$ . Since  $\varphi_1$  and  $\varphi_2$  are linearly independent and  $\Psi^*(-x, y) = \gamma \Psi(x, y)$ , we deduce that  $c_2^* = \gamma c_1$  and  $c_1^* = \gamma c_2$  and this implies that  $|c_1| = |c_2|$  since  $|\gamma| = 1$ .

## A.2. Field at the band edge

A special case occurs when  $k_x$  is at the edge of the (one-dimensional) BZ edge. For lossless PCs,  $k_x d = \pi$  and  $k_x d = -\pi$  are equivalent. The field  $\Psi^*(x, y)$  is then also a waveguide mode associated with  $k_x$  and  $d/\lambda$  and if  $\Psi(x, y)$  is non-degenerate then there exist  $\gamma \in \mathbb{C}$  such that  $|\gamma| = 1$  and  $\Psi^*(x, y) = \gamma \Psi(x, y)$ . Let  $\hat{\gamma}$  be a square root of  $\gamma$ , then  $\hat{\gamma} \Psi(x, y)$  is a real since

$$\Psi^*(x, y) = \hat{\gamma}^2 \Psi(x, y) \Leftrightarrow \Psi^*(x, y) = \frac{\hat{\gamma}}{\hat{\gamma}^*} \Psi(x, y) \Leftrightarrow (\hat{\gamma} \Psi(x, y))^* = \hat{\gamma} \Psi(x, y). \quad (46)$$

We can then consider the chosen mode  $\Psi(x, y)$  to be real. As a consequence, the dominant term  $(c_1 \varphi_1(x, y) + c_2 \varphi_1^*(-x, y))$  must have real values. This implies that  $c_1$  and  $c_2$  are real since, as discussed in Sect. A.3,  $\varphi_1(x, y)$  can be chosen to be real if it is non-degenerate. Since  $|c_1| = |c_2|$  we then have  $c_2 = \pm c_1$ . The choice  $c_2 = -c_1$  cancels the field  $(c_1 \varphi_1(x, y) + c_2 \varphi_1^*(-x, y))$  along  $x = 0$ , but this would contradict the fact that in Fig. 2, the component  $E_y$  is strong around the

cylinder center  $(x, y) = (0, 0)$ . Thus we must have  $c_2 = c_1$ . When translating the bulk lattice vector  $\mathbf{e}_2$ ,  $\ell$  times, we acquire a Bloch factor

$$\mu_1^\ell = e^{-i\ell k_x d/2} e^{-i\ell \beta_1 d \sqrt{3}/2} e^{\ell \kappa_1 d \sqrt{3}/2} = (-i)^\ell (-i)^\ell e^{\ell \kappa_1 d \sqrt{3}/2} = (-1)^\ell e^{\ell \kappa_1 d \sqrt{3}/2} \quad (47)$$

$$\mu_2^\ell = e^{-i\ell k_x d/2} e^{i\ell \beta_1 d \sqrt{3}/2} e^{\ell \kappa_1 d \sqrt{3}/2} = (-i)^\ell (i)^\ell e^{\ell \kappa_1 d \sqrt{3}/2} = e^{\ell \kappa_1 d \sqrt{3}/2} \quad (48)$$

and the corresponding dominant field is

$$c_1 (\varphi_1((x, y) - \ell \mathbf{e}_2) + \varphi_2((x, y) - \ell \mathbf{e}_2)) = c_1 (\mu_1^\ell \varphi_1(x, y) + \mu_2^\ell \varphi_2(x, y)) \quad (49)$$

$$= c_1 e^{\ell \kappa_1 d \sqrt{3}/2} \left( (-1)^\ell \varphi_1(x, y) + \varphi_1(-x, y) \right) \quad (50)$$

For all odd  $\ell$ , the field cancels at the cylinder centers on the row  $y = -\ell \sqrt{3}/2$  and the coupling goes to zero for all odd causing the degeneracy seen in Fig. 2(c).

### A.3. Properties of the phase factor at the band edge

When  $k_x d = \pi$ ,  $\varphi(x, y)$ ,  $\varphi(-x, y)$ ,  $\varphi^*(x, y)$  and  $\varphi^*(-x, y)$  are all permissible Bloch modes, i.e., they satisfy the same quasi-periodicity condition with respect to the lattice vector  $\mathbf{e}_1$ . They are associated with the wave vectors  $\mathbf{k} = [\pm k_x, \pm \beta + i \kappa]$ . Since  $\exp(\pm i k_x d/2) = \pm i$ , the wave vectors  $\mathbf{k} = [\pm k_x, \pm \beta + i \kappa]$  correspond to at least two different phase factors  $\mu$  [see Eq. (44)]. Indeed we have the three situations

1. If  $\exp(-i \beta d \sqrt{3}/2) = \exp(i \beta d \sqrt{3}/2)$ , i.e., if  $(\beta d \sqrt{3}/2)$  is a multiple of  $\pi$ , then we have a pair of opposite pure complex phase factors. We have  $\varphi^*(-x, y) = \gamma \varphi(x, y)$ , with  $\gamma \in \mathbb{C}$ , if there is no degeneracy.
2. If  $\exp(-i \beta d \sqrt{3}/2) = -\exp(i \beta d \sqrt{3}/2)$ , i.e., if  $(\beta d \sqrt{3}/2) \equiv \pm \pi/2$ , then we have a pair of opposite real phase factors. We have  $\varphi^*(x, y) = \gamma \varphi(x, y)$ , with  $\gamma \in \mathbb{C}$ , if there is no degeneracy; furthermore, by following the arguments used for Eq. (46), it turn out that  $\varphi(x, y)$  can be chosen as a real valued function.
3. If  $\exp(-i \beta d \sqrt{3}/2) \neq \pm \exp(i \beta d \sqrt{3}/2)$ , then we have quadruple Bloch factors  $\mu$ ,  $-\mu$ ,  $\mu^*$  and  $-\mu^*$ .

Our numerical calculations confirm the occurrence of the first two cases; in the first gap of the hexagonal lattice, the dominant eigenvalues  $\mu_1$  and  $\mu_2$  are a pair of opposite real numbers while some higher order eigenvalues form a pair of opposite imaginary complex numbers. However we have not observed the last case, with quadruple evanescent modes having the same decay.

### Acknowledgements

The authors thank P.Y. Chen and Dr A.A. Sukhorukov for useful discussions. Support of the Australian Research Council through its Centres of Excellence Program is acknowledged.